Mean flow and fluctuations in the three-dimensional turbulent cellular flow

S. Berti●

Univ. Lille, ULR 7512, Unité de Mécanique de Lille Joseph Boussinesq (UML), 59000 Lille, France

G. Boffetta●*

*Dipartimento di Fisica and INFN, Università degli Studi di Torino, via P. Giuria 1, 10125 Torino, Italy
and Okinawa Institute of Science and Technology, 1919-1 Tancha, Onna-son, Okinawa 904-0495, Japan*

S. Musacchio

Dipartimento di Fisica and INFN, Università degli Studi di Torino, via P. Giuria 1, 10125 Torino, Italy

We study, by means of extensive direct numerical simulations, the turbulent flow
produced by a two-dimensional cellular forcing in a cubic box with periodic boundary
conditions. We find that, in spite of the developed turbulence that recovers isotropic
features at small scales, the signature of forcing remains in the mean flow (averaged over
time and over the homogeneous direction). This allows us to introduce a friction factor,
whose dependence on the Reynolds number is investigated. We further show that the flow
is characterized by large temporal fluctuations of the total energy, as a consequence of the
exchange between the forced mean flow at large scales and turbulent fluctuations at small
scales. Such temporal fluctuations produce a correction to the energy spectrum that can be
explained by a simple dimensional argument.

I. INTRODUCTION

Theoretical and numerical studies of turbulent flows can be divided into two broad categories.
The first class of studies, mainly motivated by experiments and practical applications, considers
turbulence as generated by the interaction of the flow with a solid object. The most studied example
is the case of turbulence produced at the boundaries of a container, as in channel and pipe flows or
in Taylor-Couette flow [1,2]. The second category focuses mainly on intrinsic, bulk properties of
turbulence far from boundaries, which may be expected to give universal statistics independently of
the way the flow is generated. These studies are usually based on the simplest possible geometry in
the absence of boundaries, the so-called homogeneous-isotropic turbulence in periodic domains.

Between these two widely studied flows, there is space for another group of inhomogeneous and
anisotropic flows in the absence of boundaries. In this case, homogeneity and isotropy are broken
not by physical boundaries, but by the body force that sustains the flow. An important class in this
group is that of forces able to produce a stationary laminar flow, balanced by the viscous term,
which is a solution of the Navier-Stokes equation. The most studied examples in this class are the
Kolmogorov flow [3,4], the Taylor-Green vortex [5,6], and the Arnold-Beltrami-Childress flow [7].

In this work, we consider another important instance in this class, namely the cellular flow
produced by a two-dimensional, two-component periodic forcing that does not depend on the third
(vertical) dimension. At low Reynolds (Re) number, the laminar flow consists of a regular array of

---

*Corresponding author: guido.boffetta@unito.it

counter-rotating vortices. At high Re values, the laminar solution is unstable, and the flow produced by the cellular forcing becomes turbulent.

We investigate the properties of the cellular flow in the turbulent regime at different Reynolds numbers, focusing on the structure of the mean flow and on the statistical properties of the spatial and temporal velocity fluctuations. We show that the mean velocity field, averaged in time and in the vertical direction, is almost monochromatic and it reflects the spatial structure and symmetry of the forcing field. This remarkable property allows us to define a friction factor based on the vorticity budget, which is equivalent to the friction factor based on the momentum budget in the case of the Kolmogorov flow [4]. As in wall-bounded flows, the friction factor quantifies the (inverse) efficiency of the work done by the external force to sustain the mean flow.

Besides the mean flow, we also investigate the statistics of the turbulent fluctuations, discussing the recovery of isotropy at small scales and the relevance of turbulent velocities in the vertical direction, orthogonal to the mean flow. Finally, we discuss the impact of the temporal fluctuations, which are due to the turbulent dynamics. In particular, we find that the kinetic energy and the energy dissipation rates display strong fluctuations in time which are correlated with strong variations of the mean-flow intensity. Such oscillatory behavior corresponds to an alternation of phases in which the flow displays dominant two-dimensional (2D) and three-dimensional (3D) structures [8]. The presence of these temporal fluctuations induces a correction to the kinetic energy spectrum, whose form can be explained by a dimensional argument.

In addition to its theoretical interest, which is due to the simple structure of the mean flow, the cellular flow also represents a useful idealized model for geophysical applications [9,10]. For instance, the present configuration may have some relevance for ocean turbulence, where large (mesoscale) coherent eddies, characterized by essentially horizontal motions, populate the flow together with smaller (submesoscale) turbulent features displaying much more important vertical velocities. In spite of the idealized nature of the cellular flow in comparison with realistic oceanographic conditions, its settings may provide useful to gain insight into the basic mechanisms controlling the effect of turbulence on the transport of inert or chemical and biological tracers in ocean flows.

This article is organized as follows. In Sec. II we introduce the model and the simulation settings. Section III reports the results about the statistical properties of turbulence in this flow. The properties of the mean vorticity field are discussed in Sec. III A, and the role of temporal fluctuations in Sec. III B. Finally, discussions and conclusions are presented in Sec. IV.

II. MODEL AND NUMERICAL SIMULATIONS

We consider the 3D Navier-Stokes (NS) equation for an incompressible velocity field $\boldsymbol{u}(\boldsymbol{x}, t)$, written for the vorticity field $\boldsymbol{\omega} = \nabla \times \boldsymbol{u}$ as

$$\partial_t \boldsymbol{\omega} + \boldsymbol{u} \cdot \nabla \omega = \boldsymbol{\omega} \cdot \nabla u + \nu \nabla^2 \boldsymbol{\omega} + \nabla \times \boldsymbol{f}_u, \tag{1}$$

where ν is the kinematic viscosity, and $\boldsymbol{f}_u = (-F \sin(Ky), F \sin(Kx), 0)$ is the 2D, two-component body force. The NS equation admits in this case the laminar steady solution for the velocity $\boldsymbol{u}_0 = (-U_0 \sin(Ky), U_0 \sin(Kx), 0)$ and vorticity $\boldsymbol{\omega}_0 = (0, 0, U_0 K[\cos(Kx) + \cos(Ky)])$ with $U_0 = F/(\nu K^2)$. This solution is called *cellular flow* because it has the form of a regular array of vortices with alternating circulation sign. By rotating the reference frame of an angle $\theta = \pi/4$ around the z axis, i.e., with the coordinate transformation $\tilde{x} = (y + x)\sqrt{2}/2$, $\tilde{y} = (y - x)\sqrt{2}/2$, $\tilde{z} = z$, and by rescaling the wave number as $\tilde{K} = K\sqrt{2}/2$, the cellular flow can be written in the equivalent form $\boldsymbol{\omega}_0(\tilde{x}, \tilde{y}, \tilde{z}) = (0, 0, 2\sqrt{2}U_0\tilde{K}[\cos(\tilde{K}\tilde{x})\cos(\tilde{K}\tilde{y})])$, which corresponds to the 2D stationary Taylor-Green vortex [5]. The laminar solution of the cellular flow is linearly stable when $\mathrm{Re} = U_0/(\nu K) \leqslant \mathrm{Re}_c = 2\sqrt{2}$ [11]. For $\mathrm{Re} > \mathrm{Re}_c$, the basic flow develops large-scale perturbations that, increasing the Reynolds number, become chaotic [12], and eventually, for $\mathrm{Re} \gg \mathrm{Re}_c$, the flow becomes 3D and turbulent.

In the following, we consider the situation $\mathrm{Re} \gg \mathrm{Re}_c$ for which no analytic approach is available, and we therefore exploit direct high-resolution numerical simulations of the NS equations. To this

TABLE I. Parameters of the simulations: F is the forcing amplitude, E is the mean kinetic energy, u_x and u_z are the rms value of the x and z velocity components, respectively, U is the amplitude of mode $(k_x, k_y) = (0, 1)$ of $\overline{u_x}(x, y)$ (see the text), $\mathrm{Re} = U/(\nu K)$ is the Reynolds number, $R_\lambda = [10E'^2/(3Z')]^{1/2}/\nu$ is the Taylor-based Reynolds number (where $E' = E - U^2/2$ is the turbulent kinetic energy and Z' is the turbulent enstrophy), $\varepsilon = \nu \langle (\nabla \boldsymbol{u})^2 \rangle$ is the mean energy dissipation, $\eta = (\nu^3/\varepsilon)^{1/4}$ is the Kolmogorov scale, $\tau_\eta = (\nu/\varepsilon)^{1/2}$ is the Kolmogorov timescale, and $T = E/\varepsilon$ is the integral timescale. The forcing wave number $K = 1$ and the viscosity $\nu = 10^{-3}$ are fixed for all simulations. The spatial resolution is $N = 256$ for runs up to $F = 0.04$, and $N = 512$ for larger F. For all simulations, $k_{\max} \eta \geqslant 1.17$.

F	E	u_x	u_z	U	Re	R_λ	ε	η	τ_η	T
0.005	0.032	0.16	0.11	0.17	165	82	8.3×10^{-4}	3.3×10^{-2}	1.1	39
0.01	0.071	0.24	0.15	0.25	249	105	2.5×10^{-3}	2.5×10^{-2}	0.64	28
0.02	0.16	0.36	0.22	0.38	375	129	7.5×10^{-3}	1.9×10^{-2}	0.37	21
0.04	0.29	0.49	0.31	0.50	500	149	2.0×10^{-2}	1.5×10^{-2}	0.22	15
0.08	0.57	0.69	0.44	0.68	681	177	5.5×10^{-2}	1.2×10^{-2}	0.13	10
0.16	1.24	1.01	0.65	1.03	1030	222	0.166	8.8×10^{-3}	0.077	7.5
0.32	2.36	1.39	0.90	1.40	1400	258	0.450	6.9×10^{-3}	0.047	5.2

aim, we use a fully dealiased, pseudospectral code that integrates Eq. (1) on a periodic cubic domain of side $L = 2\pi$ at resolution N^3. We fixed the forcing wave number to $K = 1$ and the viscosity to $\nu = 10^{-3}$, so that the only control parameter is the forcing amplitude F. For each value of F, we perform a bootstrap simulation to reach a statistically stationary state, followed by very long simulations (over 25–100 eddy-turnover-times, depending on F) during which average quantities are computed. Table I reports the main parameters of the simulations.

Figure 1 shows two examples of the z component of the vorticity field for the run at $F = 0.04$ at two different instants of time, corresponding to a maximum (left) and a minimum (right) of the global kinetic energy (see Fig. 2). It is evident that the flow is fully turbulent with positive and negative vorticity structures, which appear elongated mostly along the homogeneous direction z, in

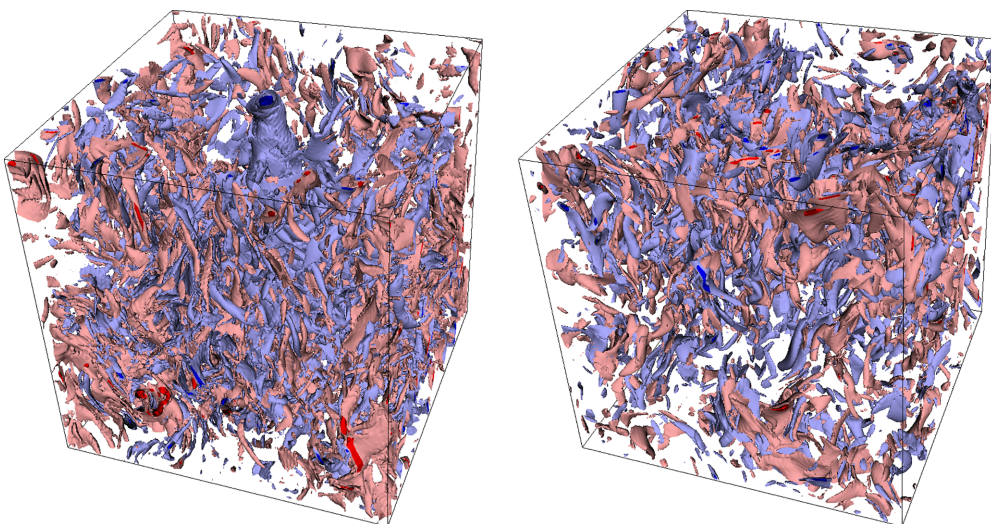FIG. 1. Snapshots of the vertical vorticity field for the simulation with $F = 0.04$ at two different times ($t = 200$ on the left and $t = 800$ on the right) corresponding to a maximum and a minimum of kinetic energy. Blue (red) regions correspond to positive (negative) values of $\omega_z(\boldsymbol{x}, t)$.
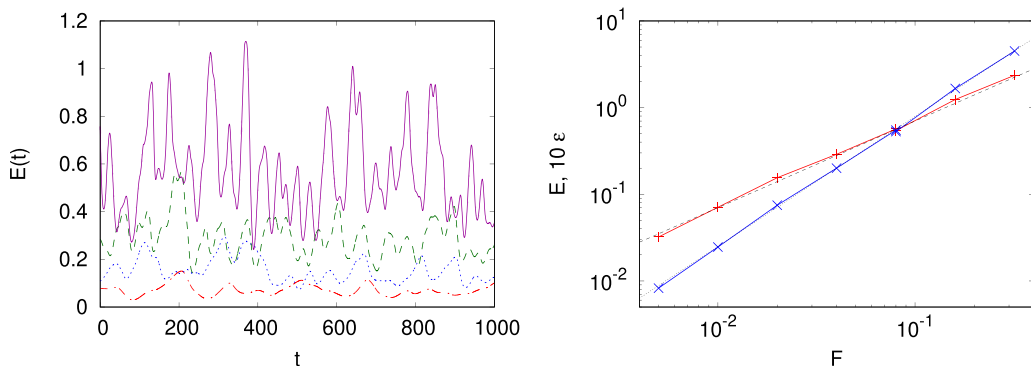
FIG. 2. Left panel: Kinetic energy $E(t)$ as a function of time for simulations with $F = 0.01$ (red dot-dashed line), $F = 0.02$ (blue dotted line), $F = 0.04$ (green dashed line), and $F = 0.08$ (purple continuous line). Right panel: Time-averaged kinetic energy (red line, plus symbols) and energy dissipation rate (blue line, cross symbols) as a function of the forcing amplitude F. The dashed (dotted) line has slope 1 (3/2). The energy dissipation rate has been rescaled by a factor 10 for clarity.

particular for the high-energy case (left panel in Fig. 1), where a large-scale vortex at the center of the computational box is observable.

III. STATISTICS OF THE TURBULENT FLOW

Figure 2 (left panel) shows the time evolution of the mean kinetic energy $E = \frac{1}{2}\langle|\boldsymbol{u}|^2\rangle$, where $\langle\cdots\rangle = 1/L^3 \int \cdots d^3x$ is the average over the whole domain, for a set of simulations in statistically stationary conditions. We observe large fluctuations in the instantaneous value of the energy, with characteristic time proportional to the integral timescale $T = E/\varepsilon$ of the flow. Because of these oscillations, very long simulations are required in order to reach the convergence of the statistical quantities.

The time-averaged values of the energy E and of the energy dissipation rate $\varepsilon = \nu\langle(\nabla\boldsymbol{u})^2\rangle$ increase with the forcing amplitude F, as shown in Fig. 2 (right panel). Scaling predictions for E and ε can be derived by simple dimensional arguments. The energy balance reads $\dot{E} = -\varepsilon + \langle\boldsymbol{f}_u \cdot \boldsymbol{u}\rangle$, where the dot stands for the time derivative, and the last term is the energy injection rate of the deterministic forcing. In stationary conditions the time derivative vanishes, and using the dimensional estimations $\langle\boldsymbol{f}_u \cdot \boldsymbol{u}\rangle \simeq FE^{1/2}$ and $\varepsilon \simeq E^{3/2}K$, we obtain the scaling predictions $E \propto F$ and $\varepsilon \propto F^{3/2}$. Both of these scaling laws are observed in our simulations (see Fig. 2, right panel).

At large scales, the turbulent cellular flow is anisotropic, as a consequence of the forcing, which acts on the horizontal components of the velocity only. This is shown by the ratio of the vertical to the horizontal root-mean-square (rms) velocity u_z/u_x, which is close to 0.65 for all the values of the forcing amplitude F (see Fig. 3). Nonetheless, the ratio of the vertical to the horizontal rms vorticity ω_z/ω_x (which is dominated by small-scale contributions) remains close to unity, suggesting that isotropy is recovered at small scales. Moreover, the ratios u_y/u_x and ω_y/ω_x, which are close to unity for all the values of F, indicate that the flow is statistically isotropic in the (x, y) plane.

The instantaneous one-dimensional (1D) energy spectra of the x and z components of the velocity field are shown in Fig. 4. The 1D energy spectra $E_i(k_j)$ are computed by taking the Fourier transform of the ith component of the velocity field along the jth direction, and then by averaging the resulting square amplitude over the other two directions.

At large scale, the 1D spectrum of horizontal velocity [e.g., $E_x(k_y)$ in the left panel of Fig. 4] reveals the presence of strong, anisotropic flow at $k_y = 1$, which is absent in the vertical component $E_z(k_y)$ (right panel of Fig. 4). Such an energy peak is observed in the transverse horizontal mode, i.e., $k_y = 1$ for E_x and $k_x = 1$ for E_y. This reflects the vortical structure of the large-scale flow.
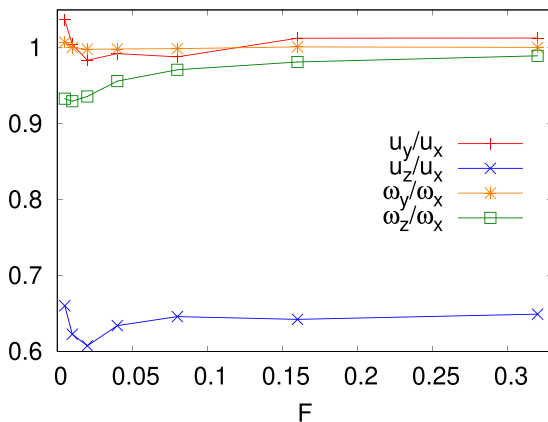
FIG. 3. Ratio of the rms values of velocity and vorticity components as a function of the forcing amplitude F.

Nonetheless, the spectra recover isotropy at small scales (i.e., at wave numbers $k \gtrsim 10$) with values of the ratios $E_z(k_x)/E_x(k_z)$, $E_z(k_y)/E_x(k_y)$, and $E_z(k_z)/E_x(k_x)$ close to 1 (Fig. 4, right inset). The spectra of the y component of the velocity (not shown) are indistinguishable from that of the x component (exchanging k_x with k_y).

At intermediate scales, the turbulent cascade develops a Kolmogorov spectrum $E(k) = C\varepsilon^{2/3}k^{-5/3}$ for both the components E_x and E_z. From the Kármán relation [13] between the second-order transverse and longitudinal structure functions, which holds under the hypotheses of statistical homogeneity and isotropy, it is possible to derive a prediction for the 1D spectra in the transverse and longitudinal modes $E_\perp(k) = [E_{||}(k) - k\partial_k E_{||}(k)]/2$. Our results show that the transverse spectra $E_y(k_x)$ and $E_z(k_x)$ are in good agreement with the prediction $E_{y,z}(k_x) = [E_x(k_x) - k_x\partial_{k_x}E_x(k_x)]/2$ at high wave numbers (see the inset of Fig. 4, left panel). This is further confirmation of the recovery of isotropy at small scales.

We remark that a systematic study of the anisotropy of the turbulent flow can be done on the basis of the irreducible representation of the rotational symmetry SO(3) group [14]. This more sophisticated approach, which is beyond the scope of the present paper, has demonstrated that
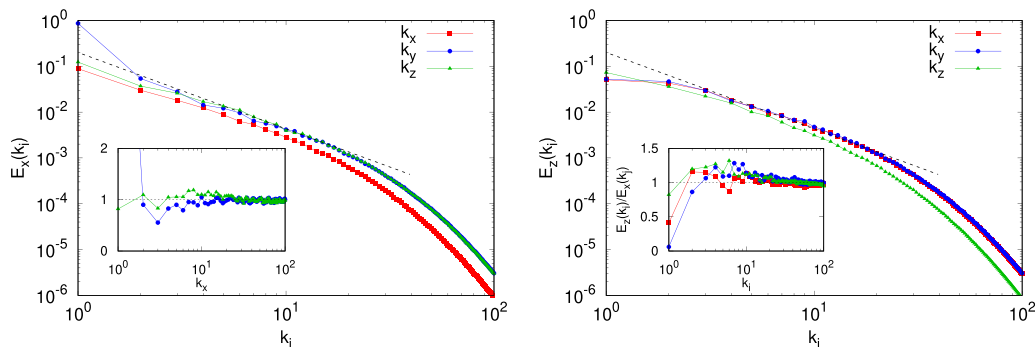

FIG. 4. One-dimensional energy spectrum for the x (left panel) and z (right panel) components of the velocity field as a function of the wave numbers k_x (red squares), k_y (blue circles), k_z (green triangles), for the run with $F = 0.32$. The dashed line represents the Kolmogorov scaling $E(k) \sim \varepsilon^{2/3}k^{-5/3}$. Inset, left: ratios $E_y(k_x)/[E_x(k_x)/2 - k_x\partial_{k_x}E_x(k_x)/2]$ (blue circles) and $E_z(k_x)/[E_x(k_x)/2 - k_x\partial_{k_x}E_x(k_x)/2]$ (green triangles). Inset, right: ratios $E_z(k_x)/E_x(k_z)$ (red squares), $E_z(k_y)/E_x(k_y)$ (blue circles), and $E_z(k_z)/E_x(k_x)$ (green triangles).
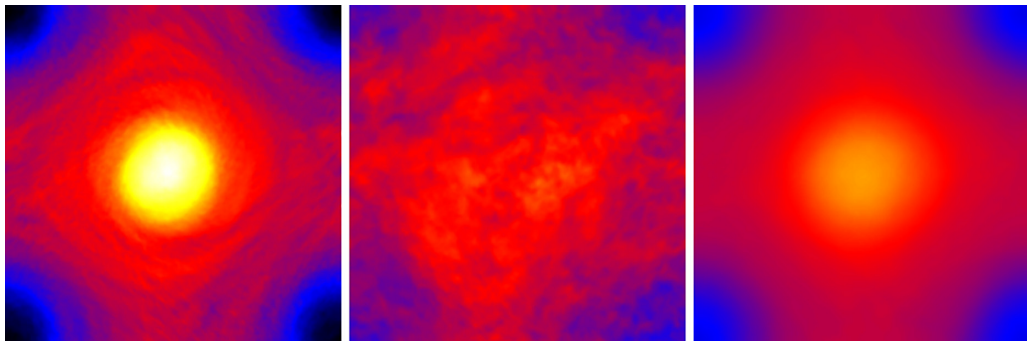
FIG. 5. Snapshots of the vertical vorticity $\overline{\omega_z}(x, y)$ averaged over the homogeneous z direction, from the run at $F = 0.04$. Black (white) corresponds to maximally negative (positive) vorticity. Left (center): time $t = 200$ ($t = 240$) corresponding to a maximum (minimum) of the kinetic energy. Right: temporal average.

different anisotropic sectors of a turbulent flow display different scaling exponents and that, in general, the isotropic sector dominates at small scales [15].

A. Mean vorticity field

In spite of the complexity of the vorticity field shown in Fig. 1, it is remarkable that it is possible to recover the structure of the inhomogeneous forcing by computing the average of the fields over the homogeneous direction z, which we denote as $\overline{(\cdots)} = (1/L) \int_0^L (\cdots) dz$. Figure 5 shows that the vertically averaged vorticity field $\overline{\omega_z}(x, y)$ displays a clear signature of the forcing. We also observe the presence of strong temporal fluctuations in the instantaneous fields $\overline{\omega_z}$ computed at different times. The fluctuations of $\overline{\omega_z}$ are correlated with those of the energy, observed in Fig. 2. Maxima of the energy occur when the flow displays a strong 2D vortical structure, while weak 2D structures correspond to the minima of energy. The quasiperiodic alternation of these phases had been already noted in a previous numerical study [8], and it is a consequence of the cellular forcing, which accumulates energy in the 2D large-scale flow, until the latter is discharged through the turbulent cascade, which is an intrinsically 3D process.

When the vorticity field is averaged also over time, it becomes almost monochromatic, with a spatial structure equal to that of the laminar solution (with a different amplitude $U \neq U_0$), i.e., $\overline{\omega_z}(x, y) \simeq UK[\cos(Kx) + \cos(Ky)]$ (see Fig. 5). This remarkable feature is observed also in other turbulent flows forced by monochromatic forcing, such as the Kolmogorov flow [4]. The 2D spectral analysis of $\overline{\omega_z}(x, y)$, reported in Fig. 6, shows that the square amplitude of the first subleading modes $(k_x, k_y) = (1, 2)$ and $(k_x, k_y) = (2, 1)$ is about 3% of that of the leading modes $(k_x, k_y) = (0, 1)$ and $(k_x, k_y) = (1, 0)$. The modes with $k > 3$ have essentially negligible amplitude. Figure 6 (right panel) shows that this property is almost independent on the Reynolds number of the flow.

We now consider the vorticity budget. In statistically stationary conditions, by taking the vertical average of the z-component of Eq. (1), one obtains

$$\partial_x \overline{u_x \omega_z} + \partial_y \overline{u_y \omega_z} - \partial_x \overline{\omega_x u_z} - \partial_y \overline{\omega_y u_z} - \nu(\partial_x^2 + \partial_y^2)\overline{\omega_z} = KF[\cos(Kx) + \cos(Ky)] \qquad (2)$$

and similar equations for the other two components (without the forcing term, which has the z component only).

In the laminar regime, the first two terms on the left-hand side of the equation (advection terms) sum to zero, the vortex stretching terms vanish identically, and Eq. (2) reduces to the balance between the forcing and the viscous term, which gives the relation for the amplitudes $F = \nu K^2 U_0$. In analogy with [4], we define the friction factor $f \equiv F/(KU^2)$, which represents the inverse of the efficiency of the work done by the forcing to produce the coherent vortical motion. At $\mathrm{Re} < \mathrm{Re}_c$, the friction factor follows the viscous scaling $f = \nu K/U_0 = 1/\mathrm{Re}$.
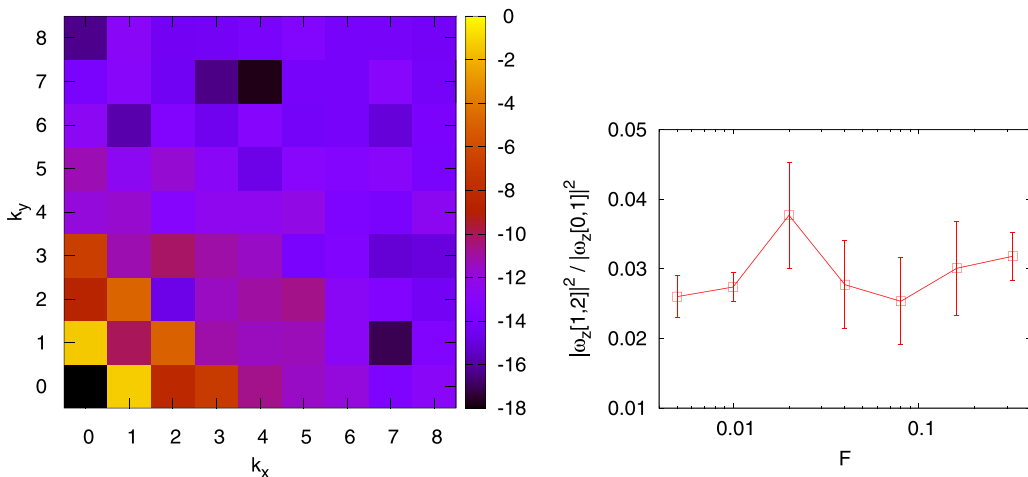
FIG. 6. Left: Two-dimensional spectrum of the vertical vorticity $\overline{\omega_z}(x, y)$ averaged over the homogeneous direction z and time, for the run at $F = 0.16$. The range of wave numbers is limited to $0 \leqslant k_i \leqslant 8$ ($i = x, y$). Colors are log-scaled. Right: Ratio of the square spectral amplitude of mode [1,2] of the vertical vorticity to the square amplitude of the dominant mode [0,1] as a function of the forcing intensity F.

In the turbulent regime ($\mathrm{Re} \gg \mathrm{Re}_c$) the contribution of the dissipative term in Eq. (2) becomes negligible, and the forcing is balanced by the quadratic terms. These terms have a complex structure, given by the superposition of several modes beyond the basic mode of the forcing. This is an important difference with respect to the case of the Kolmogorov parallel flow where the Reynolds stress has a simple monochromatic profile [4]. Nonetheless, given that the cellular forcing is monochromatic, it is interesting to consider the contributions of the leading Fourier components, associated with the wave numbers $(k_x, k_y) = (0, 1)$ and $(k_x, k_y) = (1, 0)$ where the forcing acts, of the different terms to the vorticity budget. The inset of Fig. 7 shows the relative contribution to the vorticity budget of the quadratic terms in Eq. (2). These correspond to the sum of the amplitudes of the modes $(k_x, k_y) = (0, 1)$ and $(k_x, k_y) = (1, 0)$ from either the advection terms $\overline{u_i \omega_z}$ or the vortex-stretching ones $\overline{\omega_i u_z}$ (with $i = x, y$), normalized by the amplitude of the forcing F. Independently of F, we find that the main contribution (about 80%) to the vorticity budget, Eq. (2), comes from the advection term $\boldsymbol{u} \cdot \nabla \omega$, while the vortex stretching term $\boldsymbol{\omega} \cdot \nabla u$ only accounts for the remaining 20%.

The friction factor is shown in the main plot of Fig. 7 as a function of the Reynolds number. The error bars are estimated here from the temporal fluctuations of the amplitude U of the modes $(k_x, k_y) = (0, 1)$ and $(k_x, k_y) = (1, 0)$ of the velocity field. These fluctuations correspond to the alternation of configurations with strong and weak mean flow (see Fig. 5). Although the statistical uncertainty on the values of f is quite large (in particular for the simulation at lower Re), we observe that at high Re the friction factor fluctuates around an almost constant value $f \approx 0.16 \pm 0.02$. This is in agreement with the dimensional scaling $U \sim E^{1/2} \sim F^{1/2}$, which is suggested by the results of Fig. 2. We remark that the asymptotic value $f \approx 0.16$ is not far from that obtained for the Kolmogorov flow $f \approx 0.12$ [4].

B. Temporal fluctuations

Although the turbulent flow is statistically stationary, it displays strong fluctuations in time, which are evident by comparing the fields $\overline{\omega_z}(x, y)$ at different times (Fig. 5), as well as by looking at the instantaneous values of the kinetic energy (Fig. 2). Together with the kinetic energy, also the energy dissipation rate ε is affected by important fluctuations. This is shown in Fig. 8, which
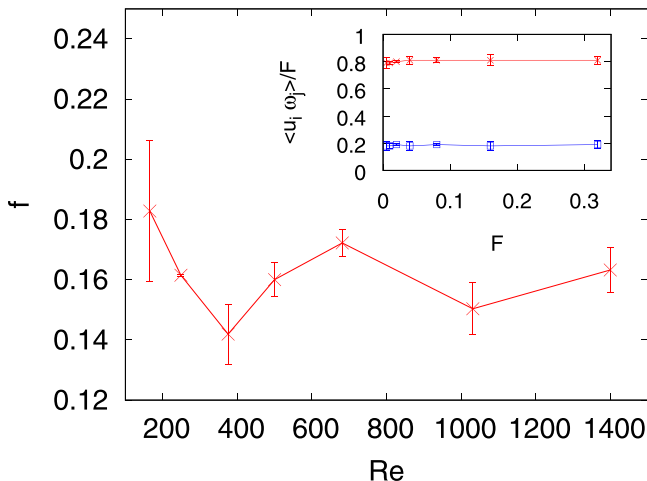
FIG. 7. Friction factor $f = F/(KU^2)$ as a function of the Reynolds number Re $= U/(\nu K)$. Errors are estimated from the fluctuations of the amplitude of the average velocity profile. Inset: relative contribution of the quadratic terms to the momentum budget of Eq. (2), normalized by the forcing amplitude. The red upper line corresponds to the contribution from the advection terms $\overline{u_i \omega_z}$, the blue lower one to that from the vortex stretching terms $\overline{\omega_i u_z}$.

reports a subset of the full time series of $E(t)$ and $\varepsilon(t)$ for the simulation at $F = 0.08$. As expected, the evolution of $\varepsilon(t)$ is correlated to that of $E(t)$, with a time delay corresponding to the time for a fluctuation produced at large scale by the forcing to reach the smallest scale where it is dissipated by viscosity. We measure this time lag from the maximum of the correlation function between energy and dissipation, defined as $C(\tau) = \int E(t)\varepsilon(t + \tau)dt$ [defined for $\tau > 0$ since $\varepsilon(t)$ is retarded with respect to $E(t)$]. The inset of Fig. 8 shows that the delay time τ computed in our simulations scales as the integral timescale $T = E/\varepsilon \simeq F^{-1/2}$. The presence of quasiperiodic
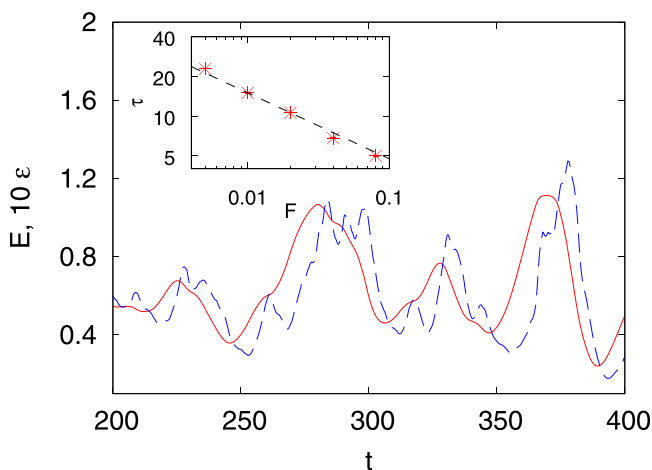

FIG. 8. Kinetic energy E (red continuous line) and energy dissipation ε (blue dashed line) as a function of time for the simulation with $F = 0.08$. For clarity, ε has been rescaled by a factor 10. Inset: correlation time between energy and dissipation (defined from the maximum of the correlation function; see the text) as a function of F. The dashed line represents the dimensional scaling $F^{-1/2}$.

oscillations of $E(t)$ and $\varepsilon(t)$, with a $\pi/2$ phase delay, had been previously reported [8]. We also note that the occurrence of maxima and minima of the energy is correlated with the sign of the time derivative of $\varepsilon(t)$. In particular, the maxima of $E(t)$ occur when $\dot{\varepsilon}(t) > 0$, while the minima of $E(t)$ occur when $\dot{\varepsilon}(t) < 0$. Indeed, by deriving with respect to time the energy balance relation, one has $\ddot{E} = -\dot{\varepsilon} + d\langle \boldsymbol{f}_u \cdot \boldsymbol{u} \rangle / dt$. In the extrema of the energy, we have $d\langle \boldsymbol{f}_u \cdot \boldsymbol{u} \rangle / dt \simeq F\dot{E}E^{-1/2} = 0$, and therefore $\dot{\varepsilon} \simeq -\ddot{E}$.

The strong fluctuations of the global quantities (such as E and ε) observed in the turbulent cellular flow have an effect also on the energy spectra. Theoretical studies of unsteady turbulence performed with a two-scale direct-interaction approximation method [16] and with the multiple-scale perturbation method [17] predicted that the temporal variation of the energy dissipation rate $\varepsilon(t)$ produces a correction to the Kolmogorov energy spectrum. This result can be obtained by simple heuristic arguments [18], starting from the time evolution of the energy spectrum [13]

$$\partial_t E(k, t) = P(k, t) - \partial_k \Pi(k, t) - D(k, t), \tag{3}$$

where $\Pi(k, t)$ is the energy flux of the turbulent cascade, $P(k, t)$ is the production spectrum due to the external force, and $D(k, t) = 2\nu k^2 E(k, t)$ is the viscous dissipation spectrum. In the inertial range, the dissipation and production terms can be neglected, therefore a steady energy spectrum (independent on t) leads to a constant energy flux (independent on k).

Now, let us assume that the energy dissipation rate $\varepsilon(t)$ varies slowly in time. We expand the energy spectrum as $E(k, t) = E_0(k, t) + E_1(k, t)$, where the first-order correction $E_1(k, t)$ is assumed to be small compared to $E_0(k, t)$ and of the same order of the time-derivative $\partial_t E_0(k, t)$. Using a dimensional estimate [19] for the energy flux $\Pi(k, t) = Ck^{5/2}E(k, t)^{3/2}$, where C is a constant, we obtain at first order

$$\Pi(k, t) = C_0^{-3/2}k^{5/2}E_0(k, t)^{3/2}\left(1 + \frac{3}{2}\frac{E_1(k, t)}{E_0(k, t)}\right) = \Pi_0(k, t) + \Pi_1(k, t), \tag{4}$$

with $C_0 = C^{-2/3}$.

Inserting (4) into (3), we get at the leading order $0 = -\partial_k \Pi_0(k, t)$, which implies that the energy flux is constant in the inertial range and it is equal to the energy dissipation rate $\Pi_0(k, t) = C_0^{-3/2}k^{5/2}E_0(k, t)^{3/2} = \varepsilon(t)$. The corresponding energy spectrum has the Kolmogorov form

$$E_0(k, t) = C_0\varepsilon(t)^{2/3}k^{-5/3}. \tag{5}$$

Using (5) in the first-order expansion of (3), $\partial_t E_0(k, t) = -\partial_k[(3/2)\Pi_0(k, t)E_1(k, t)/E_0(k, t)]$, and assuming a power-law form for the correction $E_1(k, t) \sim k^\beta$, we obtain the prediction for the first-order spectral correction

$$E_1(k, t) = C_1\varepsilon(t)^{-2/3}\dot{\varepsilon}(t)k^{-7/3}, \tag{6}$$

where $C_1 = (2/3)C_0^2$. The ratio $E_1(k, t)/E_0(k, t) = (2/3)C_0\varepsilon(t)^{-4/3}\dot{\varepsilon}(t)k^{-2/3} = (2/3)C_0\tau_k/\tau_\varepsilon$ shows that the first-order expansion is justified if the timescale $\tau_\varepsilon = \varepsilon(t)/\dot{\varepsilon}(t)$ is longer than the eddy turnover time $\tau_k = \varepsilon(t)^{-1/3}k^{-2/3}$. We note that the argument for the exponent $-7/3$ of the spectral correction is independent of the specific choice of the closure for the energy transfer in terms of the energy spectrum [17,18,20–22]. Conversely, the relation between the constant C_0 and C_1 depends on the closure.

The fact that the sign of the correction $E_1(k, t)$ depends on the time derivative of ε has a simple physical interpretation. When $\dot{\varepsilon} > 0$, the forcing accumulates energy in the large-scale modes. This is evident in Fig. 8, which shows that the maxima of the energy occur at times for which $\dot{\varepsilon} > 0$. This produces a steepening of the energy spectrum, which is in agreement with a positive sign of the correction $E_1(k, t)$. On the contrary, the decrease of the energy dissipation rate ($\dot{\varepsilon} < 0$) occurs immediately after strong dissipation events, during which a large amount of energy is removed from the large scales and it is transferred to the viscous scales. This results in a flattening of the energy spectrum, in agreement with a negative sign of the correction $E_1(k, t)$.
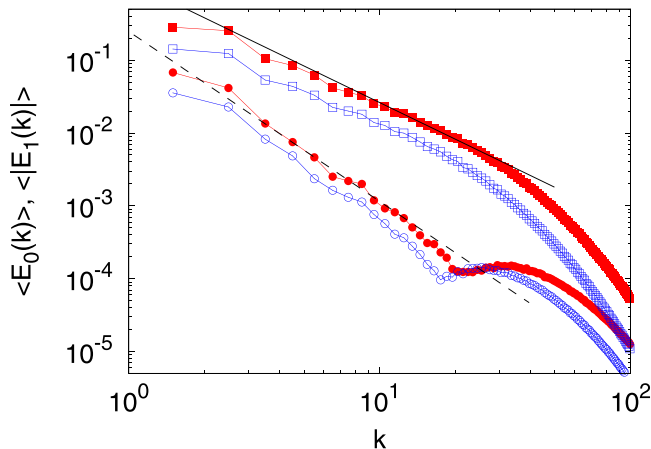
FIG. 9. Leading-order energy spectrum $\langle E_0(k,t)\rangle_t$ (squares) and spectral correction $\langle |E_1(k)|\rangle_t$ (circles). Red full symbols are for the case $F = 0.32$, blue empty symbols for $F = 0.16$. The continuous line is the spectrum $C_0\langle \varepsilon^{2/3}\rangle_t k^{-5/3}$ with $C_0 = 2.1$, the dashed line represents $C_1\langle \varepsilon^{-2/3}|\dot{\varepsilon}|\rangle_t k^{-7/3}$ with $C_1 = 2.8$.

In the case of the turbulent cellular flow considered here, even though $\varepsilon(t)$ fluctuates in time, the flow is statistically stationary on timescales much longer than the integral scale $T = E/\varepsilon$. This implies that the time average $\langle (\cdots) \rangle_t$ of the correction $E_1(k,t)$ is zero, because (6) can be written as a total time derivative $E_1(k,t) = \partial_t[3C_1\varepsilon(t)^{1/3}k^{-7/3}]$. More generally, in turbulent flows that are statistically stationary on timescales much longer than τ_ε, we have $\langle E_1(k,t)\rangle_t = 0$ and $\langle E(k,t)\rangle_t = \langle E_0(k,t)\rangle_t$, which determines the relation $C_0 = C_k\langle \varepsilon(t)\rangle_t^{2/3}/\langle \varepsilon(t)^{2/3}\rangle_t$ between C_0 and the Kolmogorov constant C_k. The constant C_1 of the correction spectrum can be obtained from the average of the absolute value, i.e., $C_1 = k^{7/3}\langle |E_1(k,t)|\rangle_t/\langle \varepsilon(t)^{-2/3}|\dot{\varepsilon}(t)|\rangle_t$.

To extract the subleading spectral correction $E_1(k,t)$ in our numerical simulations, we proceed as follows. First, we compute the time average of the instantaneous energy spectra multiplied by $\varepsilon(t)^{-2/3}$, i.e., $\langle E(k,t)\varepsilon(t)^{-2/3}\rangle_t = \langle E_0(k,t)\varepsilon(t)^{-2/3}\rangle_t + \langle E_1(k,t)\varepsilon(t)^{-2/3}\rangle_t$. The time average of the term $E_1(k,t)\varepsilon(t)^{-2/3}$ is zero since it can be written as a total time derivative $E_1(k,t)\varepsilon(t)^{-2/3} = \partial_t[-3C_1\varepsilon(t)^{-1/3}k^{-7/3}]$. Therefore, we have $\langle E(k,t)\varepsilon(t)^{-2/3}\rangle_t = \langle E_0(k,t)\varepsilon(t)^{-2/3}\rangle_t = C_0 k^{-5/3}$. This allows us to obtain the leading-order spectrum

$$E_0(k,t) = \varepsilon(t)^{2/3}\langle E(k,t)\varepsilon(t)^{-2/3}\rangle_t \tag{7}$$

and the subleading correction

$$E_1(k,t) = E(k,t) - \varepsilon(t)^{2/3}\langle E(k,t)\varepsilon(t)^{-2/3}\rangle_t. \tag{8}$$

We remind the reader that the expressions (7) and (8) are valid only for flows, which are statistically stationary over long times.

In Fig. 9 we show the time-averaged leading-order spectrum $\langle E_0(k,t)\rangle_t$, which displays the Kolmogorov scaling $k^{-5/3}$, and the absolute value of the subleading correction, averaged over time, $\langle |E_1(k,t)|\rangle_t$, which displays a clear $k^{-7/3}$ scaling, in agreement with Eq. (6). We note that the scaling range increases with Re. The measured value of the coefficient of the spectrum is $C_0 = 2.1 \pm 0.2$ (which corresponds to $C_k \simeq 2.05$), while the subleading spectrum gives $C_1 \simeq 2.8 \pm 0.4$, which is consistent with the relation obtained in (6).

The argument that leads to (6) takes into account the temporal fluctuations of the flow, while it assumes statistical homogeneity in space. This is justified in the case of the cellular flow, because the spatial fluctuations are weaker than the temporal ones. A theory that accounts for the presence of spatial inhomogeneities has been recently proposed [23] for the turbulent Kolmogorov flow, in which the spatial fluctuations are comparable or even stronger than the temporal ones. Interestingly,

the prediction for the spectral correction arising from the inhomogeneities of the flow, derived under the assumption of statistical stationarity, has the same scaling exponent $-7/3$ of the nonstationary case discussed here. Hence, for the cellular flow, a refined theory that includes the subleading effects of the spatial inhomogeneity would not alter the scaling law of the correction term.

IV. CONCLUSIONS

We presented a series of direct numerical simulations of a turbulent, inhomogeneous flow, sustained by a two-dimensional, two-component force with a monochromatic, cellular (vortexlike) spatial structure.

Our results show that the turbulent flow retains a memory of the spatial structure of the forcing, which is recovered by averaging the vorticity field along the vertical homogeneous direction and/or over time. As a consequence, the mean flow has basically the same form of the laminar solution, except for a reduced amplitude. This property allows us to define a friction factor, in analogy with the case of wall-bounded flows, which quantifies the intensity of the force that is necessary to sustain a mean flow with given kinetic energy. Our results show that the friction factor approaches a constant value at large Re, consistently with dimensional predictions.

In addition to the time-averaged statistical properties, we find that the turbulent cellular flow displays strong temporal fluctuations. Its dynamics are characterized by an alternation of phases in which the 2D forcing accumulates kinetic energy in the large-scale flow, followed by phases in which the energy is rapidly transferred toward the small dissipative scales by the 3D turbulent cascade process. In the "energy charging" phase, the flow displays a marked 2D structure, which is the hallmark of the forcing. Conversely, the 2D mean flow is weaker in the "discharging" phases, which are characterized by intense energy dissipation rates. The temporal fluctuations of the dissipation rates affect also the spectral properties, causing the appearance of a correction to the Kolmogorov energy spectrum, with subleading spectral exponent $-7/3$, in agreement with theoretical predictions [16,17].

We conclude by noting that the turbulent cellular flow can offer an ideal configuration to study the spreading of tracer or inertial particles in an inhomogeneous turbulent flow for, e.g., applications to pollutant dispersion and plastics sedimentation [24], one of the big challenges in environmental fluid dynamics [25], avoiding ad hoc small-scale parametrizations. It can also be instructive for other Lagrangian advection studies, which are often considered to assess the effect of unresolved velocity components, but rely on kinematic or essentially laminar flows [10]. Similarly, for fundamental studies, it may reveal interesting information about the role of turbulence in plankton dynamics, particularly in relation to nutrient upwelling [26,27] and to the different assumptions of the biological modeling. Along a similar line of reasoning, it can be noted that cellular-flow patterns (with vortical motions on the vertical) also appear in Langmuir circulation [28,29], a distinctive feature of the ocean mixed-layer dynamics with important implications on marine ecology. Starting from the basic fluid-dynamical equations, a reduced, kinematic model of such motions was obtained [28,30,31], which essentially coincides with the laminar solution of the flow considered here. Therefore, the present setup may also be useful to explore how the survival conditions of phytoplankton are affected by the simultaneous presence of large-scale advection and small-scale turbulent motions in (Langmuir) convective flows [32–34].

[1] M. Avila, D. Barkley, and B. Hof, Transition to turbulence in pipe flow, Annu. Rev. Fluid Mech. **55**, 575 (2023).

[2] S. Grossmann, D. Lohse, and C. Sun, High–Reynolds number Taylor-Couette turbulence, Annu. Rev. Fluid Mech. **48**, 53 (2016).

[3] L. Meshalkin and I. Sinai, Investigation of the stability of a stationary solution of a system of equations for the plane movement of an incompressible viscous liquid, J. Appl. Math. Mech. **25**, 1700 (1961).

[4] S. Musacchio and G. Boffetta, Turbulent channel without boundaries: The periodic Kolmogorov flow, Phys. Rev. E **89**, 023004 (2014).

[5] G. I. Taylor and A. E. Green, Mechanism of the production of small eddies from large ones, Proc. R. Soc. London A **158**, 499 (1937).

[6] M. E. Brachet, D. I. Meiron, S. A. Orszag, B. Nickel, R. H. Morf, and U. Frisch, Small-scale structure of the Taylor–Green vortex, J. Fluid Mech. **130**, 411 (1983).

[7] V. I. Arnold, Sur la topologie des écoulements stationnaires des fluides parfaits, in *Vladimir I. Arnold-Collected Works* (Springer, 1965), pp. 15–18.

[8] S. Goto, Y. Saito, and G. Kawahara, Hierarchy of antiparallel vortex tubes in spatially periodic turbulence at high Reynolds numbers, Phys. Rev. Fluids **2**, 064603 (2017).

[9] A. Majda and X. Wang, *Nonlinear Dynamics and Statistical Theories for Basic Geophysical Flows* (Cambridge University Press, 2006).

[10] G. L. Forgia, D. Cavaliere, S. Espa, F. Falcini, and G. Lacorata, Numerical and experimental analysis of Lagrangian dispersion in two-dimensional chaotic flows, Sci. Rep. **12**, 7461 (2022).

[11] G. Sivashinsky and V. Yakhot, Negative viscosity effect in large-scale flows, Phys. Fluids **28**, 1040 (1985).

[12] P. Perlekar and R. Pandit, Turbulence-induced melting of a nonequilibrium vortex crystal in a forced thin fluid film, New J. Phys. **12**, 023033 (2010).

[13] G. K. Batchelor, *The Theory of Homogeneous Turbulence* (Cambridge University Press, 1953).

[14] L. Biferale and I. Procaccia, Anisotropy in turbulent flows and in turbulent transport, Phys. Rep. **414**, 43 (2005).

[15] I. Arad, L. Biferale, I. Mazzitelli, and I. Procaccia, Disentangling Scaling Properties in Anisotropic and Inhomogeneous Turbulence, Phys. Rev. Lett. **82**, 5040 (1999).

[16] A. Yoshizawa, Nonequilibrium effect of the turbulent-energy-production process on the inertial-range energy spectrum, Phys. Rev. E **49**, 4065 (1994).

[17] S. L. Woodruff and R. Rubinstein, Multiple-scale perturbation analysis of slowly evolving turbulence, J. Fluid Mech. **565**, 95 (2006).

[18] W. J. T. Bos and R. Rubinstein, Dissipation in unsteady turbulence, Phys. Rev. Fluids **2**, 022601(R) (2017).

[19] L. S. Kovasznay, Spectrum of locally isotropic turbulence, J. Aeronaut. Sci. **15**, 745 (1948).

[20] R. Rubinstein and T. T. Clark, Self-similar turbulence evolution and the dissipation rate transport equation, Phys. Fluids **17**, 095104 (2005).

[21] W. J. Bos, Production and dissipation of kinetic energy in grid turbulence, Phys. Rev. Fluids **5**, 104607 (2020).

[22] K. Steiros, Turbulence near initial conditions, Phys. Rev. Fluids **7**, 104607 (2022).

[23] R. Araki and W. J. Bos, Inertial range scaling of inhomogeneous turbulence, arXiv:2210.14516.

[24] A. Baudena, E. Ser-Giacomi, I. Jalón-Rojas, F. Galgani, and M. L. Pedrotti, The streaming of plastic in the Mediterranean Sea, Nat. Commun. **13**, 2981 (2022).

[25] T. Dauxois, T. Peacock, P. Bauer, C. P. Caulfield, C. Cenedese, C. Gorlé, G. Haller, G. N. Ivey, P. F. Linden, E. Meiburg, N. Pinardi, N. M. Vriend, and A. W. Woods, Confronting grand challenges in environmental fluid mechanics, Phys. Rev. Fluids **6**, 020501 (2021).

[26] K. Guseva and U. Feudel, Numerical modelling of the effect of intermittent upwelling events on plankton blooms, J. R. Soc. Interface **17**, 20190889 (2020).

[27] M. Freilich, G. Flierl, and A. Mahadevan, Diversity of growth rates maximizes phytoplankton productivity in an eddying ocean, Geophys. Res. Lett. **49**, e2021GL096180 (2022).

[28] A. D. D. Craik and S. Leibovich, A rational model for Langmuir circulations, J. Fluid Mech. **73**, 401 (1976).

[29] S. A. Thorpe, Langmuir circulation, Annu. Rev. Fluid Mech. **36**, 55 (2004).

[30] I. M. Moroz and S. Leibovich, Competing instabilities in a nonlinear model of Langmuir circulations, Phys. Fluids **28**, 2050 (1985).

[31] M. A. Bees, Planktonic communities and chaotic advection in dynamical models of Langmuir circulation, Appl. Sci. Res. **59**, 141 (1998).

[32] J. R. Taylor and R. Ferrari, Shutdown of turbulent convection as a new criterion for the onset of spring phytoplankton blooms, Limnol. Oceanogr. **56**, 2293 (2011).

[33] C. Lindemann, A. Visser, and P. Mariani, Dynamics of phytoplankton blooms in turbulent vortex cells, J. R. Soc. Interface **14**, 20170453 (2017).

[34] V. B. Tergolina, E. Calzavarini, G. Mompean, and S. Berti, Effects of large-scale advection and small-scale turbulent diffusion on vertical phytoplankton dynamics, Phys. Rev. E **104**, 065106 (2021).